EXPERIMENTAL STUDY OF THE BURNING RATE OF SMALL-SCALE FOREST FUEL LAYERS

A. Fuentes*and J.L. Consalvi**
andres.fuentes@usm.cl
* Universidad Técnica Federico Santa María, Departamento de Industrias, Av. España 1680, Valparaíso, Chile.
** Université de Provence, IUSTI/ UMR CNRS 6595, 5 rue E. Fermi, 13453 Marseille Cedex 13, France

Abstract
An experimental study of burning rates of small-scale forest fuel layers composed of maritime pine needles is carried out by using the FM Global Fire Propagation Apparatus. Three fuel loads, corresponding to fuel volume fractions of about 0.02, 0.04 and 0.08, are exposed to external heat fluxes in the range 15-30kW/m^2. The analysis of the experimental data focuses on the flaming stage. The time evolution of the mass loss rate exhibits the same trend whatever the external radiant heat flux and the fuel load considered. Just after ignition (short time) a linear increase is observed whereas after the peak (long time) the mass loss rate follows an exponential decay with time. The flaming residence times and the characteristic times of the exponential decay are found to be weakly influenced by the external radiant heat flux and while they increase exponentially with the fuel load. A dimensional analysis suggests that the mass loss process at long time can be described by a first order Arrhenius law. The characteristic time of the exponential decay can then be interpreted as a characteristic chemical time scale, showing that the degradation process becomes slower as the fuel volume fraction increases and providing in turn a phenomenological explanation of the exponential increase in flaming residence time with the fuel load. It is also found that measured flame heights at the peak of mass loss rate are consistent with those predicted by the classical correlations of the literature. In addition, analysis of the remaining mass of solid fuel at flaming extinction shows that the char oxidation process becomes of increasing importance as the fuel volume fraction becomes larger.

Introduction
The spread of surface fires through forest fuel litters is of primarily importance in the development of wildland fires. It allows the greatest extent of fire spread [1], plays a major role in the transition from a surface fire to a crown fire and contributes to sustain the subsequent crown fire spread [2]. Typically the heat flux provided, in one hand, by the part of the flame above the fuel litter and, in another hand, by the hot combustion gases and solid particles located inside the fuel bed contributes to heat the solid fuel located ahead of the fire front up to a pyrolysis temperature. The volatiles escaping from the solid fuel mix with air and the combustible mixture is ignited by the flame, sustaining the spread process. The burning rate and the piloted ignition processes of forest fuel litters are key issues in surface flame spread. The first, which is closely related to the heat release rate (HRR), determines the air entrainment, the flame geometry and temperature [3] and is then of primarily importance to predict the heat transfer toward the unburnt fuel. The second characterizes the propensity of the fuel bed to ensure the spread process.

Recently laboratory small-scale experiments, based on calorimetric devices such as the cone calorimeter or the Fire Propagation Apparatus (FPA), were carried out to study the piloted ignition and the burning rate of forest fuel litters [4-8]. These experimental devices were widely used to characterize the flammability parameters of standard solid fuels such as polymers [9] or different species of wood [10, 11]. Wildland fuels differ from standard solid fuels since they consist in highly dilute porous media, i.e. the solid phase occupies a small fraction of the fuel bed volume. Schemel *et al.* [4] demonstrate the usefulness of calorimetric

studies to characterize the flammability of wildland fuels representative of the Mediterranean ecosystem. They considered two species of pine needles, namely *Pinus halepensis* and *Pinus pinaster*, having different shape and different surface-to-volume ratios. Tests were conducted under natural and forced flows. They demonstrated that the transport processes inside the fuel beds has a significant influence on flammability characteristics, both time to piloted ignition and HRR being widely influenced by flow conditions and fuel species. Bartoli *et al.* [5] extended this work and demonstrated that the surface-to-fuel ratio and fuel packing ratios are not the only parameters affecting the burning process, the chemical composition of the pyrolysis products having also an influence. Mindykowski et al. [7] focused on the piloted ignition process by considering fuel beds composed of different loads of maritime pine needles and kermes oak leaves exposed to different radiative flux. For the fuel beds considered they found that the inverse of the ignition time is linearly dependent on the imposed heat flux, as observed for thermally-thin solids. Consalvi et al. [8] used a physically-based two-phase model to simulate the experiments reported in [7]. They found that, for a given fuel volume fraction, the mass flow rate of combustible gases at the surface of the fuel bed at ignition is independent on the external heat flux and that this critical mass flow rate increases as the fuel volume fraction decreases.

The aim of this study is to analyze some experimental data, obtained in FPA, and relative to the burning rate of small-scale litters of maritime pine needles. Emphasis is put on the mechanisms controlling the burning rate for different external heat fluxes and fuel volume fractions.

Experimental Method

Experiments were conducted in the FM-Global Fire Propagation Apparatus (FPA) [12]. This calorimeter comprises two sections. The combustion arrangement is constituted basically of four external infrared heaters, pilot igniter, sample holder, load cell, and a data acquisition system. Figure 1 presents a schematic of the experimental set-up of the FPA. In the other part, a hood system topped the combustion zone. It has been dimensioned so that all the combustion gases are sucked up. From the hood, the system narrows to an exhaust duct to ensure gases mixing. Finally, the volumetric flow rate is measured by a Pitot tube and gases are continuously distributed to a set of different analyzers to measure O_2, CO/CO_2 concentrations.

The ignition pilot consists of an ethylene/air premixed flame. The visible region of the pilot flame was adjusted to approximately 1cm in length, with a diameter of 0.5cm. The pilot flame was located 1cm above the center of the fuel bed as shown in Figure 1. Each infrared heater contains six tungsten filament tubular quartz lamps in a compact reflector body that would be capable of providing heat fluxes to the specimen in the range of 10-100kW/m^2. In agreement with previous studies [4, 7, 8] the maximum of radiant heat flux was fixed at 30kW/m^2.

Prior to each test the total incident heat flux was calibrated using a Gardon type fluxmeter. This gauge has an accuracy of within ±3% and repeatability within 0.5% between calibrations [12]. Calibration of the total heat flux as a function of the voltage supply to the lamp was performed. Under steady irradiance the total voltage lamp is proportional to the incident heat flux. However, this relationship changes with time and therefore the abovementioned procedure was repeated before each test and was adjusted if necessary. The homogeneity of irradiance was verified using theoretical computations perform with the Monte Carlo procedure [13].

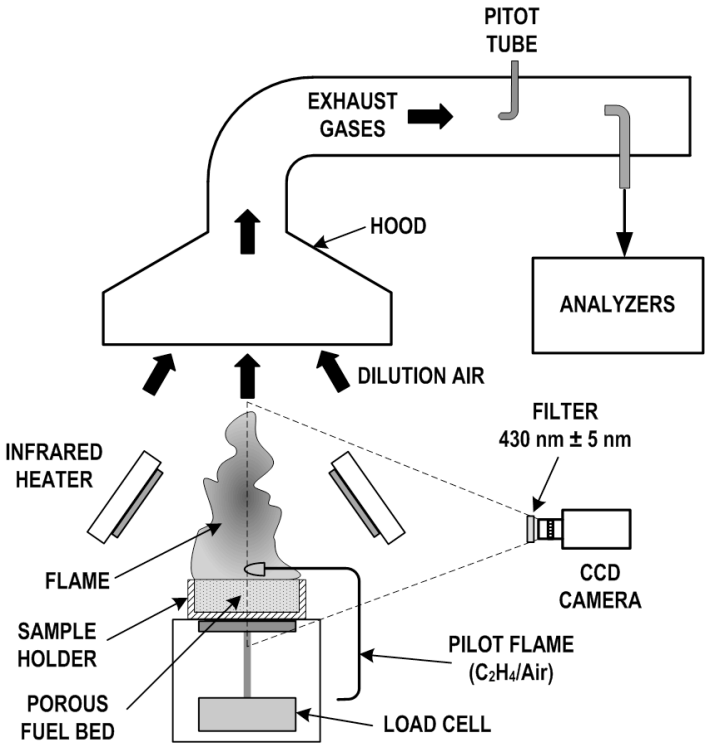

Figure 1. Schematic of the Fire Propagation Apparatus (FPA).

The flaming residence time, defined as the elapsed time between flaming ignition and extinction, was determined visually from the times of appearance and disappearance of the visible flame. Both times were recorded using a timer installed in a digital data collection system triggered by the operator. The timer is able of recording elapsed time to the nearest tenth of 1s and has an accuracy of better than 1s in 1h. Also a video verification of the flaming residence time was obtained from frames recorded by a scan monochrome CCD camera obtaining images in the visible region of the spectrum. The mass loss was also automatically recorded in the digital data collection system, with a frequency of 1Hz.

Experiments were performed following the standard FPA protocols [12]. No external wind was imposed during these measurements, and the only the airflow was that induced by the FPA blower and natural convection from the samples. The separation between the top of the fuel bed and base of the lamps was 7.3cm. After the specimen holder was placed on top of a load cell for mass measurement the position of pilot flame was adjusted. At this time the water-cooled shield was positioned between the lamps and the sample area to limit preheating and background measurements and calibration were completed. The shield was rapidly removed to expose the sample to the imposed heat flux, which defined time zero.

The specimen holder was a stainless steel basket open at the top, 12.6cm in diameter and 3cm high. Unlike the experiments of Schemel et al. [16], the side of the sample holder in this study was closed (Fig. 1). Dead wildland fuels were considered in this work, namely Maritime Pine (MP) needles. Sometimes two or three MP needles were connected together by a needle sheath, forming a fascicle. Needles generally longer than the size of the container were cut using scissors. No attempt was made to separate the sheaths from the needles. Small debris (i.e. small pieces of wood, leave or needles) were removed when encountered. The needles were randomly distributed by hand to entirely fill the basket so that the fuel volume fraction is given by $\alpha_k = m_k / \rho_k V_{basket}$. Fuel types and loadings are representative of Mediterranean forest litters [14]. Table 1 summarizes the geometrical and physical properties of the fuel beds considered in the study. Free moisture absorbed by the fuel is known to be an

important parameter for the ignition. In this study fuel elements were oven-dried at 60°C during twelve hours. After this time no further changes in mass were observed, suggesting that no moisture remains. However a weakly free moisture percentage is expected to be present in the fuel but this quantity was the same for all experiments [15].

Table 1. Physical properties of wildland fuel beds.

Fuel Type		m_k (g)	α_k	σ_k (m^{-1})	ρ_k (kg/m^3)
Maritime Pine needles	MP1	5.0	0.020	5500 [16]	630 [16]
	MP2	10.0	0.040		
	MP3	20.0	0.080		

The experimental flame height was evaluated using CH* chemiluminescence measurements from flame, with another CCD camera. This camera recorded ten side view frames per second and was mounted with a narrow band filter centered at 431 nm (10 nm FWHM). It is important to note that CH* radicals have been proved to be central to many hydrocarbon combustion chemical pathways [17], as they originate from the reaction between O_2 and C_2H. These excited radicals return to ground state either through collisional quenching or through spontaneous fluorescence, whose transition occurs at 431.4nm. Therefore, CH* chemiluminescence measurements can be directly related to the burning rate of the primary fuel [18].

A *f*/0.95 17.0mm focal length lens was mounted on each camera focused at the burner plane of symmetry. The spatial resolution of the CH* images were determined by the pixel size in the CCD matrix and the detection optics. The overall result in the present experiment was that each pixel corresponds to a region of 0.25x0.25mm. Before the determination of flame height the CH* signals were corrected for background noise and removing the devices, as the heater, affecting the image treatment. A Matlab program was developed in order to obtain a computed contour image allowing the determination of reaction zone height for each image. A representative image obtained using the technique presented above is showed in Fig. 2.

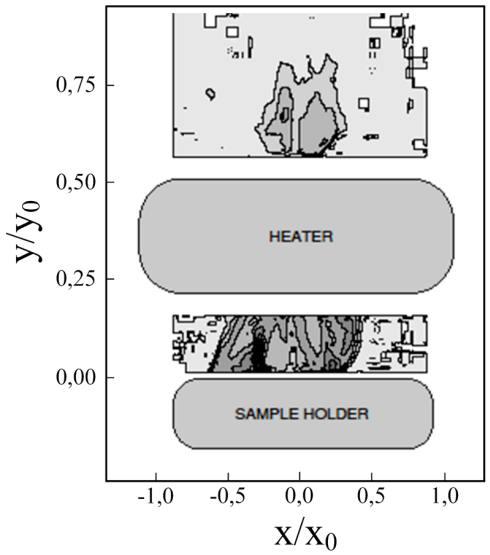

Figure 2. Typical computed image of the CH* spontaneous emission of the flame. The basket was filled with a 20g of pine needles an exposed to $20kW/m^2$.

Experimental Results

Figure 3 shows the time evolution of the mass loss rate (MLR) for a basket filled with 20g of pine needles and exposed to an external heat flux of 20kW/m^2. Typically, the time evolution of the MLR can be divided into three stages. The first stage corresponds to preheating of the fuel bed due to the radiant heat flux provided by the heaters. It is characterized by a slow increase of the MLR. The solid phase is progressively heated and begins to release volatiles. This heating and the resulting pyrolysis are non-uniform through the fuel bed due to the attenuation of the radiant heat flux by the pine needles [8]. Gaseous pyrolysis products (GPP) are transported toward the surface of the fuel bed by a flow resulting from a balance between buoyancy forces and the drag force exerted by the fuel particles. Flaming ignition occurs when a particular stoichiometry is reached at the level of the pilot and is related, for a given fuel load, to a critical mass flux of combustible gaseous species at the surface of the fuel bed, this critical mass flux being almost independent of the imposed radiant flux. In the present test flaming ignition occurs at $t=t_{ig}$=42s. The second stage is the flaming stage. Also, Figure 3 shows that flaming ignition is followed by a rapid increase in MLR since the heat transferred from the flame to the solid fuel is added to radiant contribution of the heaters. By considering the fuel bed as a control volume, the heat captured by the solid fuel due to the combustion process can be schematically decomposed into two contributions. Firstly the part of the flame located above the fuel bed contributes to heat up the fuel litter by radiation. Secondly the highly diluted nature of the fuel beds allows fresh air to be entrained into the fuel layer and to react, in one hand, with the combustible part of the pyrolysis products and, in another hand, with the char residue produced by the pyrolysis of the solid fuel. As a consequence, these homogeneous and heterogeneous combustion processes release heat inside the fuel layer which also contributes to transfer energy to the solid fuel. This pattern differs notably from that observed for standard solid fuels, such as polymers and pieces of wood, for which the radiative and convective contributions of the flame can be considered to be transferred into the solid by conduction After this sharp increase the MLR reaches a peak and decrease relatively slowly until the flame extinguishes. The flaming residence time, t_{comb}, is defined as the elapsed time between the ignition and the extinction of the flame. As the flame extinguishes, the last stage relative to the oxidation of char residue takes place. It is characterized by a relatively constant MLR of about 10^{-5}kg/s in the present example. The present study focuses on the second stage, i.e. the flaming stage.

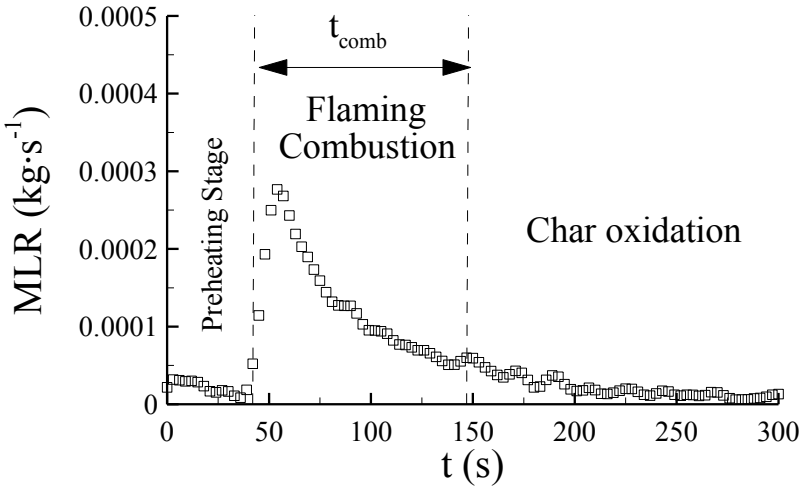

Figure 3. Time evolution of the MLR for a fuel bed using a sample holder filled with 20g of pine needles exposed to an external heat flux of 20kW/m^2.

The diagrams A, B and C in Fig. 4 show the time evolution of the MLR for fuel loads of 5, 10 and 20g respectively. Different external heat fluxes, ranging from 15kW/m^2 to 30kW/m^2, are considered. It should be pointed out that 15kW/m^2 represent the critical heat flux for ignition in the case of a fuel load of 5g [7]. For each external heat flux the data for two tests are represented in order to assess the repeatability of the experiments. The zero of the time scale is taken at flaming ignition. The three set of data exhibit a similar behavior: just after ignition (short time) the MLR increases linearly with time whereas the decay after the peak can be approximated by an exponential function. For each fuel load the linear regression at short time and the best fitting exponential-decay prediction at long time over all tests are plotted. These plots are represented in order to show the trends with no attempt of correlation. However, for a single test both linear and exponential decreasing functions match remarkably well the data at short and long time respectively. In order to complement these figures, the slope of the linear regression at short time, a, the time at which the peak occurs, t_{peak}, the corresponding value of the MLR, MLR_{peak}, and the characteristic time of the exponential decay at long time, t_c, are given in Table 1 for each experimental condition. These values are averaged over 3 tests.

Table 1. a, MLR_{peak}, t_{peak}, and t_c for the three fuel loads and radiant heat fluxes in the range 15-30kW/m^2

Fuel Load	External heat flux (kW/m^2)	a (g/s^2)	MLR_{peak} (g/s)	t_{peak} (s)	t_c (s)
5g	30	0.0427±0.0081	0.222 ±0.028	5.00±1.00	3.52±0.02
	25	0.0279E±0.0023	0.187±0.027	7.50	6.01±0.23
	20	0.0286E±0.0025	0.177±0.013	7.00±0.35	5.08±1.66
	15	0.0111±0.0028	0.115±0.030	10.00±0.74	7.56±1.90
10g	30	0.0520±0.0042	0.389±0.022	7.33±0.57	12.85±0.93
	25	0.0673±0.0045	0.460±0.011	7.75±0.97	14.71±3.57
	20	0.0543±0.0053	0.438±0.015	9.00	13.70±1.65
	15	0.0341±0.0026	0.341±0.040	11.00±0.81	10.48±0.32
20g	30	0.0325±0.0003	0.343±0.010	9.00	55.55
	25	0.0314±0.0056	0.329±0.012	11.5±1.06	50.12±3.55
	20	0.0253±0.0016	0.272±0.005	11.5±0.72	62.74±5.55
	15	0.0191±0.0035	0.270±0.028	14.5±1.12	65.12±3.37

The effects of the external heat flux, for a given fuel load, are presented in the diagrams A-C in Fig. 4 and in Table 1. As the external radiant flux decreases, the results show that, globally, t_{peak} is delayed whereas MLR_{peak} becomes lower. The values reported in Table 1 shows that a tends to decrease with the external radiant flux. The influence of the external heat flux on t_c is weak and not well pronounced (see Table 1). Figure 2D shows the evolution of the flaming residence time as function of the external heat flux for the three fuel loads considered. As expected from Figs. 2A-C the flaming residence time appears to be almost independent on the imposed radiant flux. Its averaged values over the radiant heat fluxes are of 16.04, 32, and 124.75s for fuel loads of 5, 10, and 20g respectively.

For a given incident radiant heat flux, the primarily effect of an increase in fuel load is, as expected, an increase in the flaming residence time. Fig. 2E shows that no simple relationship exists between the flaming residence times for the different fuel loads. For the fuel loads considered in this study it is found that the flaming residence times follow an exponential increase with the fuel loads. Fig 2E show also that t_c increases also exponentially with the mass of fuel bed, the rate of increase being very similar to that observed for the flaming residence times. t_c becomes larger by a factor of about 10 as the fuel load increases from 5g to 20g. The evolutions of a and MLR_{peak} exhibit a non-monotonic behavior, increasing when

the fuel load is increased from 5g to 10g but decreasing as the fuel load is increased from 10g to 20g.

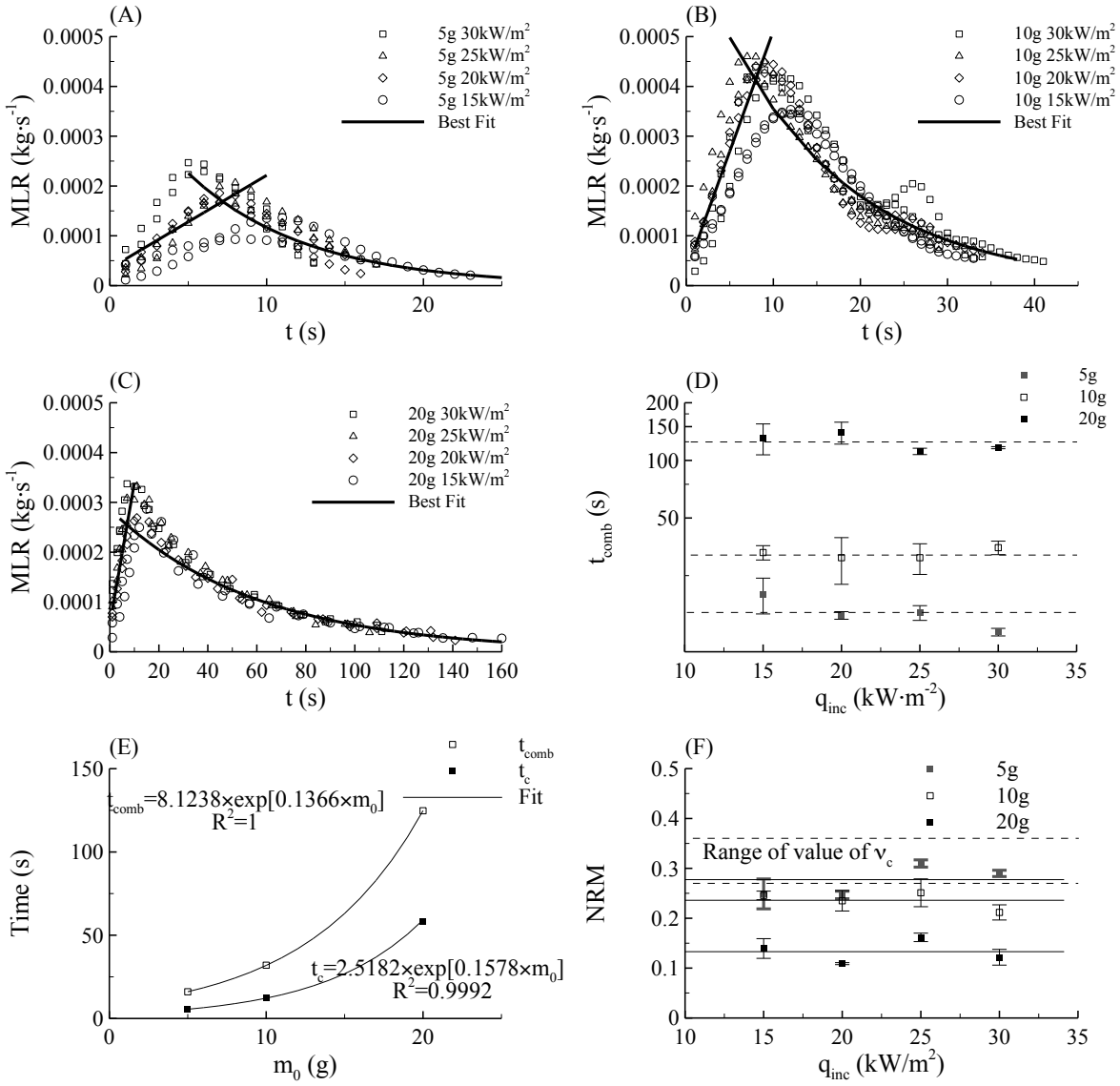

Figure 4. A) Time evolution of the MLR for fuel beds filled with 5g of pine needles and exposed to different external heat fluxes, B) same as A) but with fuel beds filled with 10g of pine needles, C) f same as A) but with fuel beds filled with 20g of pine needles, D) flaming residence time as a function of the external heat flux, E) t_{comb} and t_c as a function of the fuel load, F) normalized remaining mass at extinction as a function of the incident radiative flux. The dashed lines indicate the range of values for ν_c reported in literature for pine needles.

Figure 2F shows the normalized remaining mass (NRM) at flaming extinction. The dashed lines indicate range of values of the char content, ν_c, reported in the literature for pine needles, being between 0.27 [3] and 0.36 [2, 19]. First of all, the NRM at extinction is globally lower that the expected range of values of ν_c, which indicates that char oxidation occurs before the end of the flaming stage. This figure shows also that, for a given fuel load, the effect of the external radiant flux on the NRM at extinction are relatively weak and not well pronounced. On an opposite way it decreases significantly as the fuel load increases demonstrating that char oxidation becomes of increasing importance during the flaming stage as the fuel volume

fraction becomes higher. The averaged values of the NRM at extinction over the radiant heat flux are of 0.273, 0.236 and 0.133, for fuel loads of 5, 10, and 20g respectively.

The presence of the heaters tends to hide the flame during the test. However, flame height measurements become possible when the burning rate is sufficiently high, i.e. around the peak of mass loss rate. The available data of flame height are compared with the correlations of Heskestad [20] and of Quintiere and Grove [21]:

$$\cdot \text{Heskestad} : \dot{Q}_D^* = \left(\frac{H_{fl}/D + 1.02}{15.6} \right)^{5/2} \left(\frac{\Psi}{1-\chi_R} \right)^{3/2}$$
$$\cdot \text{Quintiere and Grove} : \dot{Q}_D^* = 0.0059 \frac{\Psi^{3/2}}{1-\chi_R} \left(\frac{H_{fl}}{D} \right)^{1/2} \left[1 + 0.357 \frac{H_{fl}}{D} \right]^2 \quad (1)$$

The normalized HRR is defined by $\dot{Q}_D^* = \dfrac{\dot{Q}}{\rho_\infty C_p T_\infty g^{1/2} D^{5/2}}$ where $\dot{Q} = \dot{m} \Delta h_c$ with $\Delta h_c = 16\text{kJ/g}$ [3]. D is the diameter of the basket. $\Psi = (1-\chi_R)\Delta h_c / s / C_p T_\infty$ where s is the stoichiometric air-to-fuel ratio and χ_R is the flame radiation fraction taken here equal to 0.25. The measurements and the correlations present an acceptable agreement. The correlation of Heskestad seems to provide a better representation of the experimental data, especially for normalized HRR lower than 0.7.

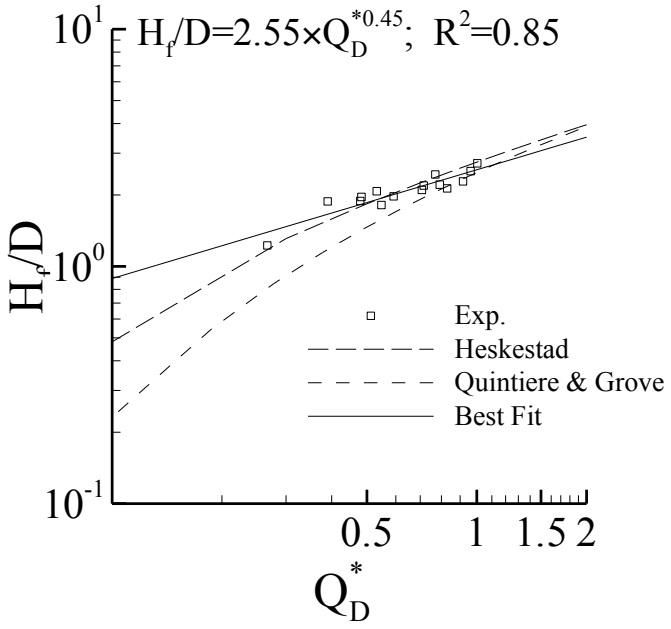

Figure 5. Dimensionless flame height as a function of the Dimensionless HRR.

Discussions

A simple analysis is developed to interpret some experimental results at longtime after the ignition of the fuel beds. During this part of the flaming stage, the exponential decay of the MLR as a function of time suggests that the global mass loss process may be described by a first order Arrhenius law. The overall fuel litters are treated as a homogeneous media undergoing a degradation process.

$$\frac{dm}{dt} = -Am\exp\left[-E/RT\right] \tag{2}$$

The following dimensionless variables are introduced:

$$\tau = t/t_{chem} \text{ with } t_{chem} = \left[A\exp(-E/RT)\right]^{-1}; m^* = \frac{m}{m_0} \tag{3}$$

where m_0 is the initial mass of pine needles. Substituting for the dimensionless variables into Eq.2 yields:

$$\frac{dm^*}{d\tau} = -m^* \tag{4}$$

Integration of Eq. 4, by considering that $m^*(\tau = 0) = 1$, gives:

$$m^* = \exp\left[-\tau\right] \tag{5}$$

The normalized mass loss rate is then expressed as:

$$\frac{dm^*}{d\tau} = -\exp\left[-\tau\right] \tag{6}$$

This analysis suggests that the characteristic times for the exponential decay, t_c, reported in Table 1 can be interpreted as the characteristic chemical time scale of the global mass loss process, t_{chem}. Figure 4A shows the normalized MLR, $MLR^* = \frac{t_{chem}}{m_0}\frac{dm}{dt}$, as a function of t/t_{chem}. The experimental data at long time represented in Figs. 2A-C are plotted in normalized coordinates in Fig. 4A. The results show that the dimensionless MLR correlates in terms of dimensionless time. Fig4. B shows the normalized flaming residence time, deduced from the correlation plotted in Fig. 4A, $-\frac{\alpha \times t_{comb}}{t_{chem}\ln\left[MLR^*_{final}/\beta\right]}$, as a function of the external radiant heat flux, where MLR^*_{final} represents the normalized MLR when the flame extinguishes and α and β are equal to 0.88033 and 0.77083 respectively. Results show that such normalization allows collapsing the flaming residence times for the three fuel loads considered. Although the physical basis of these correlations is not well understood and requires further experimental, theoretical and numerical investigations, they allows getting insights on the effect of the fuel load on the degradation process during the flaming stage. First of all, these correlations confirm that the mass loss process at long time follows a first order Arrhenius law. From Table 1, the averaged values of t_{chem}=t_c over the different radiant fluxes are of about 5.54s, 12.93 and 58.38s for fuel loads of 5, 10g and 20g respectively. The corresponding characteristic mass loss rates, m_0/t_{chem}, are then of about 0.90, 0.77, and 0.34g/s. These results show the mass loss process is widely influenced by the fuel load: as the fuel volume fraction becomes higher, the mass loss process becomes slower since the

characteristic chemical time scale increases exponentially (see Fig. 2E). This provides an explanation for the exponential increase in flaming residence time with the fuel loads.

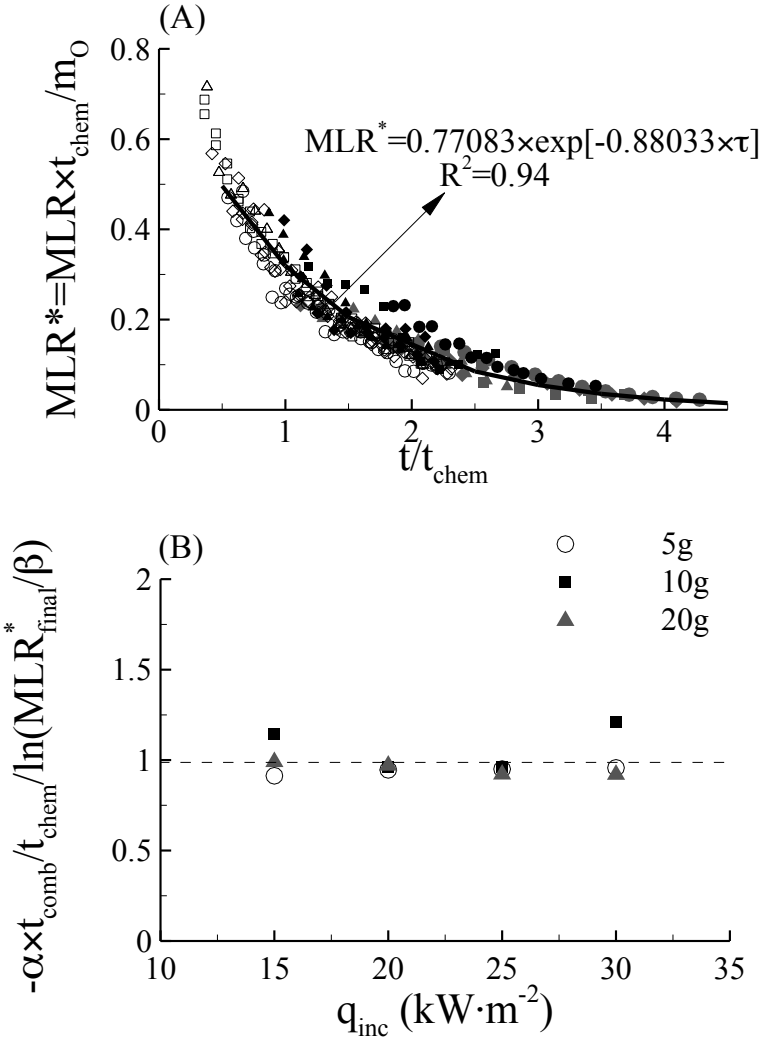

Figure 6. Longtime analysis: A) normalized MLR as a function of the normalized time for fuel loads of 5g (grey symbols), 10g (black symbols) and 20g (open symbols) and for radiant heat flux fluxes of 30kW/m^2 (squares), 25kW/m^2 (triangles), 20kW/m^2 (diamonds), and 15kW/m^2 (circles). B) Normalized flaming residence time as a function of the incident heat flux for fuel loads of 5, 10, and 20g. In the ordinate axis α=0.88033 and β=0.77083 in agreement with Fig. 6A.

Concluding Remarks

An experimental study concerning the burning rate of small-scale fuel litters composed of dry maritime pine needles was carried out by using the FM Global Fire propagation Apparatus. Three fuel loads of 5, 10 and 20g were used resulting in fuel volume fractions of 0.02, 0.04 and 0.08 respectively. External heat fluxes ranging from 15 to 30kW/m^2 are applied. The study focuses on the flaming stage. The time evolution of the mass loss rate is found to exhibit the same behavior whatever the fuel load and the radiant heat flux considered. At short time after ignition the mass loss rate increases linearly with time and reaches a peak whereas at long time an exponential decay is observed. It is shown that flame height can be evaluated by the classical correlations of the literature developed initially for pool fires and that char oxidation becomes of increasing importance as the fuel load increase. The slope of the linear

regression at short time, the location and the magnitude of the peak are influenced by both the radiant heat flux and the fuel load. On an opposite way the characteristic time scale of the exponential decay and the flaming residence time are found to be weakly dependent on the external radiant heat flux while they present an exponential increase with the fuel load. A simple analysis, based on the description of the global mass loss process by a first order Arrhenius law, is developed to interpret the experimental results at long time after ignition. From characteristic mass loss rate and time scale deduced from the analysis a correlation relating the dimensionless mass loss rate and the dimensionless time is obtained. This correlation indicates that the characteristic chemical time scale of the degradation process increases exponentially with the fuel load that provides an explanation of the exponential increase in residence time.

Phenomenological explanations of the reduction in the efficiency of the degradation process at long time as the fuel load increases can be related to the heat transferred to the solid fuel and in particular to the heat released by the homogeneous (gaseous combustion) and heterogeneous (char oxidation) combustion processes taking place inside the fuel bed. Typically an augmentation in the fuel volume fraction increases the specific area of the solid phase which reduces the permeability of the fuel beds. This may influence the flow conditions inside the fuel beds and then affects these processes. The decrease in the normalized remaining mass at extinction as the fuel load increases shown in Fig. 2F sustains this explanation. However further works are required to provide a complete understanding of these phenomena.

Acknowledgements

The authors wish to acknowledge the financial support from FONDECYT, the Chilean scientific research programme, under the project Nº1100913 and the Departamento de Industrias of the Universidad Técnica Federico Santa María. Also, the authors are thankful to the BRE Centre for Fire Protection Engineering at the University of Edinburgh for supplying the experimental apparatus FPA.

References

[1] Cohen, J.D., Finney, M.A., Yedinak, K.M., "Active spreading crown fire characteristics: Implications for modeling". In: *International Conference on Forest Fire Research*, Figueira da Foz, Portugal, 2006

[2] Grishin, A.M., *Mathematical Modeling of Forest Fires and New Methods of Fighting Them,* Pub. House Tomsk University, Tomsk, Russia*,* 1986*.*

[3] Dupuy, J.L., Meréchal, J., Morvan, D., "Fires From a Cylindrical Fuel Burner: Combustion Dynamaics and Flame Properties", Combust. Flame 135: 65-76 (2003).

[4] Schemel, C., Simeoni, A., Biteau, H., Rivera, J., Torero, J.L., "A Calorimetric Study of Wildland Fire", *Exper. Therm. Fluid Sci.* 32: 1381-1389 (2008).

[5] Bartoli, P., Simeoni, A., Biteau, H., Torero, J.L., Santoni, P.A., "Determination of the Main Parameters Influencing Forest Fuel Combustion Dynamics", *Fire Safety J.* 46: 27-33 (2011).

[6] Weise, D., White, R., Beall, F., Etlinger, M., "Use of the Cone Calorimeter to Detect Seasonal Differences in Selected Combustion Characteristics of Ornamental Vegetation", *Int. J. Wildland Fire* 14: 321-338 (2005).

[7] Mindykowski, P., Fuentes, A., Consalvi, J.L., Porterie, B., "Piloted Ignition of Wildland Fuel", *Fire Safety J.* 46: 34-40 (2011).

[8] Consalvi, J.L., Nmira, F., Fuentes, A., Mindykowski, P., Porterie, B., "Numerical Study of Piloted Ignition of Forest Fuel Layer", *Proc. Combust. Inst.* 33: 2641-2648 (2011).

[9] Rhodes, B.T., Quintiere, J.G., "Burning Rate and Flame Heat Flux for PMMA in a Cone Calorimeter", *Fire Safety J.* 26: 221-240 (1996).
[10] Spearpoint, M. J., Quintiere, J. G., "Predicting the Burning of Wood Using an Integral Model", Combust. Flame 123: 308-325 (2000).
[11] Delichatsios, M.A., Paroz, B., Bhargava, A., "Flammability Properties for Charring Materials", Fire Safety J. 38: 219-228 (2003).
[12] ASTM E2058-03, "Standard Test Method for Measurement of Synthetic Polymer Material Flammability Using a Fire Propagation Apparatus (FPA)", ASTM International, West Conshohocken, 2003.
[13] Modest, M., "Radiative Heat Transfer", Academic Press, Second Edition (2003).
[14] Pimont,F., Dupuy, J.L., Caraglio, Y., Morvan, D., "Effect of Vegetation Heterogeneity on Radiative Transfer in Forest Fires", Int. J. Wildland Fire, 18: 536–553 (2009).
[15] Manzello, S.L., Cleary, T.G., Shields, J.R., Yang, J.C. "Ignition of Mulch and Grasses by Firebrands in Wildland Urban Interface Fires", Intern. J. Wildland Fire 15: 427-431 (2006).
[16] Cohen, M., Cuiñas, P., Diez, C., Fernandes, P., Guijarro, M., Moro, C., "Wildland Fuel Particles Characterization Database Content", Fire Star Report: D6-03-A1, (2003).
[17] Najm, H.N., Paul, P.H., Mueller, C.J., Wyckoff, P.S., "On the Adequacy of Certain Experimental Observables as Measurements of Flame Burning Rate", Combust. Flame 113: 312–332 (1998).
[18] Berg, P.A., Hill, D.A., Noble, A.R., Smith, G.P., Jeffries, J.B., Crosley, D.R.,"Absolute CH* Concentration Measurements in Low Pressure Methane Flames", Combust. Flame 121: 223–235 (2000).
[19] Grishin, A.M., Sinitsyn, S.P., Akimova, I.V., "Comparative analysis of the thermokinetic constants for drying and pyrolyzing forest fuels", Combust. Expl. Shock Wave 27: 663-669 (1991).
[20] Heskestad, G., "Fire Plume Air Entrainment According to Two Competing Assumptions", Proc. Combust. Inst. 21: 111-120 (1988).
[21] Quintiere, J.G., Grove, B.S., "A Unified Analysis for Fire Plume", Proc. Combust. Inst. 27: 2757-2766 (1998).